DEVELOPMENT OF SOLAR ARRAY FOR A WIDEBAND INTERNETWORKING SATELLITE: ESD TEST

Kazuhiro Toyoda
Chiba University
Inage-ku, Chiba, JAPAN 263-8522
Phone: +81-43-290-3221
Fax: +81-43-290-3221
E-mail: toyoda@faculty.chiba-u.jp

Toshiaki Matsumoto
Yoshio Shikata
Mengu Cho
Kyushu Institute of Technology

Tetsuo Sato
JAXA (Japan Aerospace Exploration Agency)

Yukishige Nozaki
NEC TOSHIBA Space Systems, Ltd.

Abstract

This paper describes the details of ground based ESD test carried out for solar array of Wideband InterNetworking engineering test and Demonstration Satellite (WINDS).

An electron beam was used to simulate the inverted potential gradient conditions. The sustained arc was not observed for test coupons with RTV grouting at the inter-string gap and thicker RTV layer between cells and Kapton sheet. Arc pulses short-circuited the PN junction of triple-junction cells once the arcs occurred at the cell edges. Effects of exposing bus bars to space without coating with RTV were also investigated. There was no detrimental effect associated with the exposed bus bars.

Introduction

Since the last decade, the power level of Geosynchronous Orbit (GEO) satellite has increased dramatically to nearly 10 kW or even higher. To manage the large amount of power efficiently, the satellite bus voltage has increased to 100V. Nowadays many commercial telecommunication satellites employ solar arrays that generate the electricity at 100V.

As the voltage of solar array increases to 100V, the problems of arcing during the substorm condition have been recognized as serious hazard that sometimes threatens the stable supply of the solar array power. In GEO, when a satellite receives the sunlight, its charging is dominated by photoelectrons. As long as the satellite surface is well illuminated under the quiet condition, the photoelectrons keep the satellite potential within a few electron volts from the plasma potential. The insulator surface such as coverglass has similar potential. When a satellite encounters the substorm, the current due to high energy electrons increases and sometimes exceeds the current due to photoelectrons. Then the potentials of the satellite body and the insulator surface can become negative. Due to the difference of the secondary electron emission coefficients, the insulator potential may drop slower than the satellite body.

During that process, the coverglass potential can be more positive than the nearby conductor, e.g. interconnector. This situation is called "inverted potential gradient". As the potential difference builds up between coverglass and interconnector, an arc may occur.

The inverted potential gradient is the nominal case in LEO, where an arc can occur once the potential difference reaches 100 or 200 V [1]. If an arc occurs as a single pulse, it is called a trigger arc. The risk of one trigger arc growing to a catastrophic arc receiving energy from the array itself has increased recently as the power level of solar array has increased. TEMPO-2 satellite experienced the permanent loss of significant fraction of solar array output power when a severe substorm hit the satellite in 1997. The failure was attributed to an arc on solar array under the inverted potential gradient condition [2]. First, an arc occurred between adjacent array strings with different potential and short-circuited the two strings. Then the array output power of the two strings fed energy to the arc plasma. The arc current kept flowing and the underlying Kapton insulation layer was thermally broken leading to short-circuit between the array strings and the substrate. In the present paper, we call this type of sustained arc as “sustained arc”.

Since the accident of TEMPO-2, the issue of sustained arc has been investigated at several research institutions all over the world. Cho et al [3] carried out an ESD test on solar array for Engineering Test Satellite VIII (ETS8). In the laboratory test, they verified that the inverted potential gradient could occur due to the difference of secondary electron coefficients of coverglass and conductive surface. The threshold voltage for the trigger arc inception was measured to be 400V. The sustained arc between the solar array string and the CFRP substrate occurred through a defect in Kapton sheet with the potential difference of 110V and the current capability of 2.64 A. Based on the test results, precaution was taken to minimize the possibility of a defect of Kapton sheet being exposed. The thickness of RTV layer between solar cells and the Kapton sheet was increased to 70 ~ 100 μm from the originally designed value of 50 μm. In addition, RTV was leaked out from the bottom of cell to cover the Kapton sheet near interconnector.

Toyoda et al [4] found that even trigger arcs may degrade the solar array output power during the ESD test on the ETS8 solar array. Excessive coating with RTV resulted in severe contamination over coverglass surface as the amount of silicon vapor produced by trigger arc increased. Short circuit of PN junction was also observed, that decreased the string output power by the output power of one cell. The results found in Ref. [4] imply that as the number of trigger arcs accumulates in orbit, the solar array output power may decrease gradually. Historically, the effects of trigger arcs in GEO have been neglected as long as the arcs ended as pulses of finite duration. If the repeated trigger arcs truly degrade the solar array in orbit, we might have noticed it already because a trigger arc due to the inverted potential gradient can occur on any satellite regardless the bus voltage.

There are three possible explanations why we have not noticed such power degradation yet. One is that the radiation dose effect on the solar cell power degradation has been overestimated. The second one is that there have not been so many trigger arcs during the satellite lifetime to have the effect distinguishable from the radiation dose effect. The third one is that the energy of each trigger arc was not large enough to cause the degradation because the satellite power level that is proportional to the area of solar array has been low. If the third hypothesis is correct, the power degradation due to trigger arcs may emerge in near future as the size of solar array increases and the total capacitance of coverglass increases. In that case we need a model to estimate the power degradation during the satellite lifetime and

reflect the result in the design phase of satellite power system. Once a trigger arc occurs, its energy is supplied by two types of capacitance; satellite capacitance and coverglass capacitance. The satellite capacitance that is typically of the order of 100 pF is responsible for the very beginning of trigger arc inception. As the trigger arc occurs, the electrons are ejected from the arc spot and the satellite potential rapidly reaches the zero potential. Then the coverglass surface becomes positive with respect to the space plasma. The trigger arc

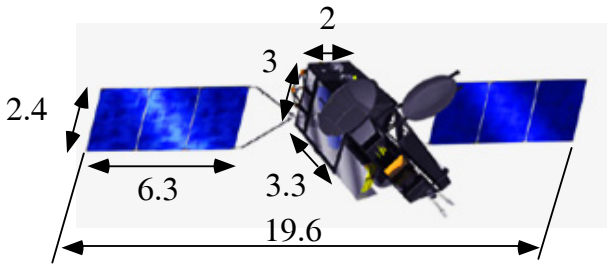

Figure 1. Artist's image of WINDS. The sizes are shown in m.

plasma neutralizes the charge stored on the coverglass and the charge flows as the arc current. Therefore, the coverglass capacitance is responsible for the growing phase of the trig ger arc. In recent high power satellites, the total amount of coverglass capacitance is 10 μF or more. With the potential difference of 1 kV between the coverglass and the solar array string, the electrostatic energy available for the trigger arc is more than 1J. Leung [5] carried out an ESD test using a very large solar array coupon (11×19 cells with the size of 30 inch by 30 inch, approximately). He observed that the trigger arc plasma expanded up to the edge of the coupon and neutralized most of the charge stored on the coverglass before the trigger arc inception.

In the present paper we report the result of ESD tests carried out on solar array for WINDS (Wideband Inter- Networking engineering test and Demonstration Satellite) that will be launched by National Space Development Agency of Japan in 2005. Figure 1 shows an artist's image of WINDS. The satellite solar array generates a power of 5.2 kW at a voltage of maximum 55 V with triple-junction cells. The satellite bus voltage is 50 V. The purposes of the test are the following;

1. Confirm that the solar array suffers no sustained arc
2. Study how the amount of RTV coating applied to the cell edge affects the power degradation due to trigger arcs
3. Determine the flight design of solar array.

The solar array design of WINDS is based on the design of ETS8 [3]. Because WINDS uses triple-junction cells instead of silicon cells used for ETS8, the difference of coverglass material might lead to a different behavior under the inverted potential gradient condition. Also, because WINDS does not carry ion thruster unlike ETS8, there is no need to coat the bus bar with RTV to avoid the current leakage to the high density plasma generated by the backflow from the ion thruster plume. We need to confirm that exposing bus bar does not give rise to new problems in terms of ESD. The power degradation found in the previous study on ETS8 [4] should be investigated further to predict the power degradation at EOL (End-of-Life). In the present paper, we first describe the test system. Then, we discuss the test result. Finally we conclude the paper by describing the flight design of solar array.

Experiment

The solar array of WINDS consists of two solar array paddles where 292 parallel strings of solar cells are mounted. Each string is made by the series connection of 30 triple-junction cells. The output voltage and currents of each string are 55 V and 0.6 A. The maximum potential difference between adjacent cells is 55 V. The coverglass is CMG-100-AR and has a thickness of 100 μm. The coverglass capacitance is 0.76 nF each. Because one paddle has approximately 4200 cells, the total coverglass capacitance is 3.2 μF for each paddle.

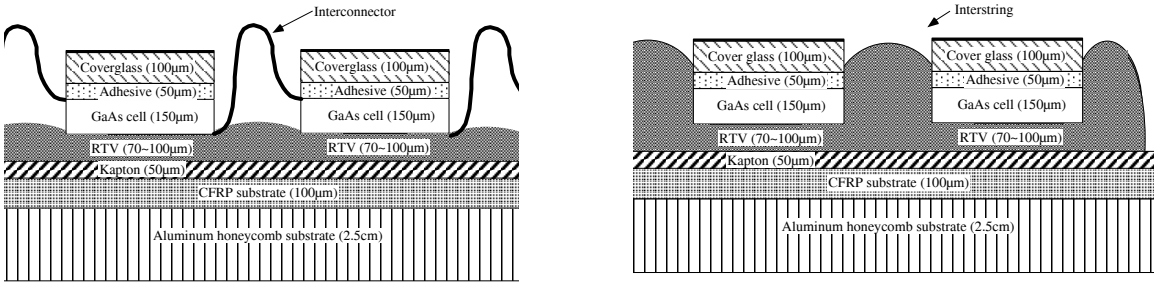

Figure 2. Cross-sectional view of coupons 2 and 3.

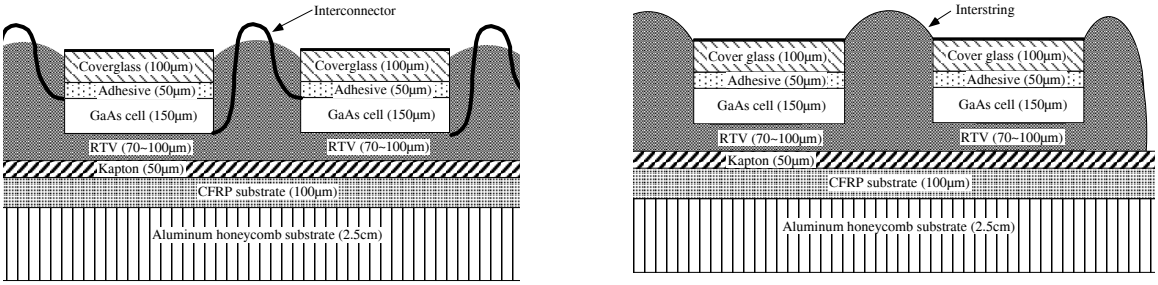

Figure 3. Cross-sectional view of coupon 1.

We used three test coupons. The cross-sectional view of solar array coupon is shown in Figs. 2 and 3. A photograph is shown in Fig. 4. The summary of difference among the coupons is listed in Table. 1. A coupon consists of 15 cells (76 mm by 37 mm each). Five cells are connected in series making three parallel strings. At the corner of each cell, a bypass-diode is attached. We name each string as R, B, and G-strings. The R- and B-strings are connected in parallel at the backside of the coupon. Therefore they always have the same potential during the ESD test. Cells are glued on Kapton sheet of 50 μm thickness with RTV silicon. The Kapton sheet is placed on top of CFRP sheet (0.1 mm thickness) and aluminium honeycomb substrate (25 mm thickness). The side of aluminium honeycomb substrate is covered by Kapton tape not to have trigger arcs.

Table 1. Difference of test coupons.

Coupon	Amount of RTV	Bass bar coating
1	large	yes
2	normal	yes
3	normal	no

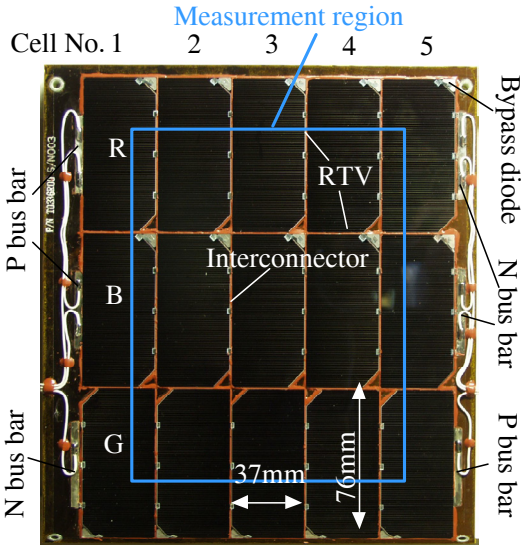

Figure 4. Photograph of a test coupon.

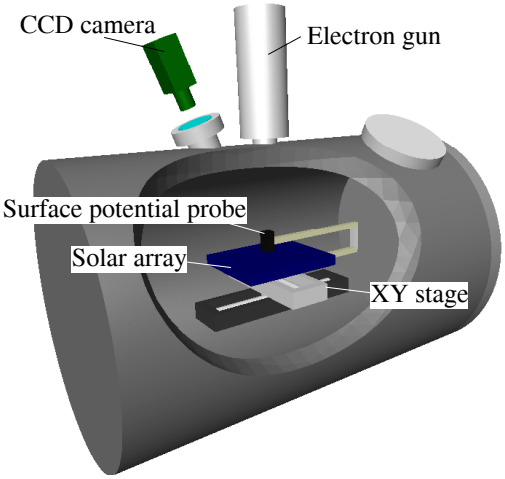

Figure 5. A schematic picture of chamber system.

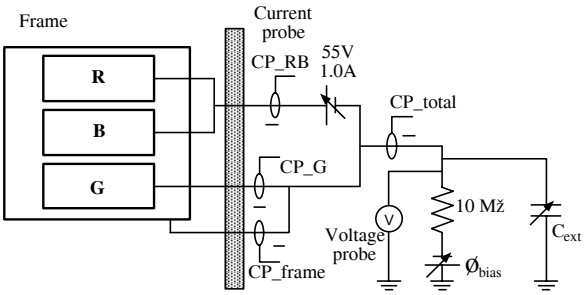

Figure 6. Layout of external circuit.

All the three coupons has the same thickness of RTV layer between cells and Kapton sheet, approximately 100 μm, inheriting the design from ETS8. The gap between strings is grouted by RTV also inheriting the design from ETS8. The coating of RTV at the cell edges of the coupon 1 is much thicker than the coating of ETS8, aiming at suppressing the trigger arc inception at the cell edges that lead to the short circuit of PN junction. The coating of RTV at the cell edges of the coupons 2 and 3 is the same as ETS8. The bus bars of the coupon 3 are not coated with RTV to save the satellite mass by a few kg. We can also expect that the bus bars act as lightning rods where a trigger arc occurs before it occurs at more dangerous points such as the string-gaps or the cell edges.

In Fig. 5, we show a schematic picture of the experiment. A coupon was placed on an acrylic plate in a vacuum chamber of 0.6m diameter and 0.9m length with the cell surface facing up. The vacuum chamber was evacuated by a turbo-molecular pomp and could reach a pressure of as low as 10^{-5} Pa before the test. During the test, the chamber pressure was 0.5 ~ 5×10^{-3} Pa. There was an electron beam gun at the top of vacuum chamber. The center of the electron beam was usually kept at the center of the coupons. The maximum beam voltage was 30 kV. At the beam energy of 3 kV that was a typical value during the test, the current density was 10 mA/m^2 and had the gaussian distribution of 150 mm diameter. The chamber

was also equipped with a Kaufman type argon plasma source that was used to remove the surface charge at the beginning of each ESD test.

A surface potential probe was attached to a XY stage to measure the two-dimensional distribution of surface potential. The surface potential probe could measure the potential up to ±20 kV. The probe moved over the coupon surface at the distance of 5mm. The probe motion was controlled by a PC and the potential was measured at the intervals of 10mm inside the area of 180mm×140mm. It took approximately 7 minutes to finish one measurement. The positions of trigger arcs were recorded by the arc position identification system [6]. The analog video image of coupon during the ESD test taken by a CCD camera was saved in real time to a PC as a digital video image sequence. After the test, the video sequence was analyzed by a computer program to identify the trigger arc positions from the optical flash associated with each trigger arc.

All the coupons were baked at 125ºC for 5 hours at the factory before they were shipped to the laboratory for the ESD tests. Other than the baking, no special treatment of the coupon surface was applied before the shipment. Once a coupon arrived at the laboratory, we first took photographs of the cell edges by ×60 optical microscope. Once a coupon was placed in the vacuum chamber and the chamber was evacuated, we baked the coupon at 70ºC ± 1ºC for 2 hours. During the ESD test, the coupon temperature was kept at 40ºC ± 1ºC.

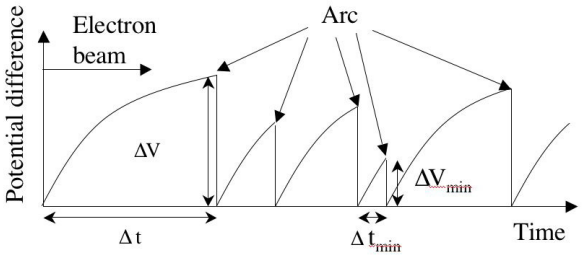

Figure 7. A schematic model of temporal profile of potential difference during the electron beam irradia-

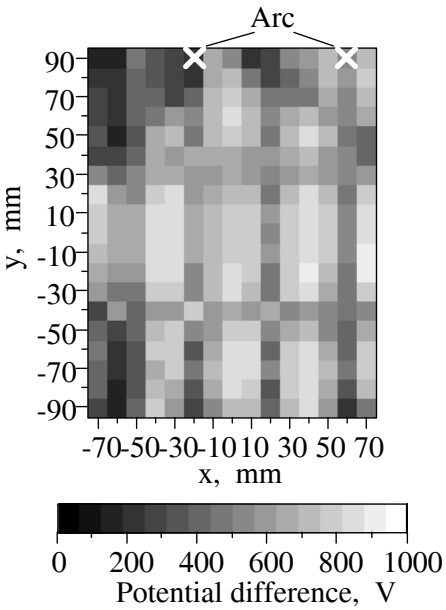

Figure 8. Distribution of potential difference at 4 s after a trigger arc inception.

In Fig. 6, we show a layout of external circuit. The coupon was electrically insulated from the vacuum chamber. The cables from the bus bars were connected to a connector at the backside of a coupon. From the connector, the cable was connected to the external circuit through high voltage feed-throughs of the vacuum chamber. The solar array coupon was biased negatively via a DC power supply. In order to protect the power supply, the resistance of 10MΩ was connected. A high voltage probe measured the potential of the coupon, $\emptyset_{bias}$. Between the R and B strings and the G string, an inter-string voltage was applied by another DC power supply. The power supply usually acted as a constant voltage source of 55 V and

would have acted as a constant current source of 1.0 A once the strings had been short-circuited by the arc plasma.

The arc current was measured via current probes. In Fig. 6, the probes denoted as CP_{RB} and CP_{total} could measure the current from DC to 10 MHz. The probes denoted as CP_{frame} and CP_G could measure from 8.5 kHz to 100 MHz. The current probes and the high voltage probes were connected to two 4 channel digital oscilloscopes (bandwidth 100MHz). The oscilloscopes were triggered once $Ø_{bias}$ increases above a certain level due to the voltage drop of the trigger arc current. The waveforms measured by the oscilloscopes were transferred to PCs via GPIB cables.

The external circuit had a capacitance to simulate the coverglass capacitance which supplied the energy to the trigger arc plasma. The value of the external capacitance was set so that the amount of electrostatic energy was equal to the energy to be given in orbit. The electrostatic energy stored in the coverglass of one solar array paddle is given by

$$U_{cg} = \frac{1}{2} C_{cg} \Delta V^2 \qquad (1)$$

where C_{cg} is the total capacitance of coverglass, 4 μF for the case of WINDS, and ΔV is the potential difference between the coverglass and the solar array string when a trigger arc occurs. The external capacitance, C_{ext}, was determined by

$$C_{ext} = \frac{2U_{cg}}{V_{bias}^{\ 2}} \qquad (2)$$

where V_{bias} was the bias voltage. In order to determine C_{ext} , we first measured ΔV before the ESD tests.

In Fig. 7 we show a schematic model of how the potential difference ΔV changes as trigger arcs occur repeatedly while the coupon is irradiated with the electron beam. We first remove the surface charge by the dense plasma generated by the plasma source. Then we irradiate the coupon with the electron beam at the constant energy and current density. The potential difference builds up as shown in Fig. 7. The potential difference follows the same temporal profile as long as the beam parameters are kept the same. At a time Δt from the start of electron beam, a trigger arc occurs at a potential difference of ΔV. Once an arc occurs, most of the coverglass charge is neutralized and the potential difference goes back to nearly zero. Because the electron beam is operated constantly, the potential difference starts to increase again immediately after the trigger arc. It is not guaranteed that the next trigger arc occurs at the same position and with the same ΔV as the previous one.

The threshold voltage for the trigger arc inception ΔV_{min} was obtained by measuring the minimum time interval between the trigger arcs, Δt_{min}. Because the real solar array consists of 4200 cells per one paddle, one cell would have the favorable conditions to arc at ΔV_{min} or less that was measured with a coupon of only 15 cells. We irradiated a solar array coupon biased to -3 kV with the electron beam of 3 keV for 1 hour. We measured the minimum time interval Δt_{min} during the one hour. Then, we irradiated the coupon with the beam and waited for an arc. Once an arc occurred, we switched off the beam at Δt_{min} from the arc inception. Then the surface potential distribution was measured to identify ΔV_{min} at the arc spot where the trigger arc occurred with the interval of Δt_{min}.

The coupon used to measure the threshold voltage ΔV_{min} was another one different from the three coupons used for the ESD test. The coupon consisted of 15 triple junction cells with CMG-100-AR coverglass. The cell layout was similar to the three ESD coupons. The only

difference from the ESD coupon was that the thickness between the cell and the Kapton sheet was 50 μm. The coupon was biased to -3 kV with an external capacitance of 100 nF. The minimum time interval was Δt_{min} = 4 sec. In Fig. 8 we show the surface potential distribution measured after the beam irradiation of 4s from an arc inception. The marks shown in Fig. 8 are the position of the arcs that had Δt_{min} = 4 sec. The maximum potential difference near the arc spot was 800 V. From this measurement we determined ΔV_{min} = 800 V. Substituting ΔV = 800 V into Eq. 1, we obtained 1.28J as the electrostatic energy given to a trigger arc. From Eq. 2 we determined C_{ext} so that the energy was close to 1.28J. During the test we used bias voltages of -3 kV, -4 kV and -6 kV. At each bias voltage we changed C_{ext} to 400 nF, 200 nF, and 100 nF to have the energy of 1.8J, 1.6J, and 1.8J.

Table 2. Test conditions.

Case	Coupon	$Ø_{bias}$, -kV	C_{ext}, nF	V_e, kV	t_{exp}, h
1	1	3	400	2.8 - 4.0	6
2	1	4	200	3.0 - 4.0	4
3	1	6	100	3.0 - 6.0	10
4	2	3	400	2.8 - 4.0	6
5	2	4	200	3.0 - 4.0	4
6	2	6	100	3.0 - 6.0	10
7	3	3	400	2.8 - 4.0	6
8	3	4	400	3.0 - 4.0	4
9	3	6	100	3.0 - 6.0	10
10	3	3	400	2.8 - 4.0	6
11	3	4	200	3.0 - 4.0	4
12	3	3	400	3.0 - 4.0	35

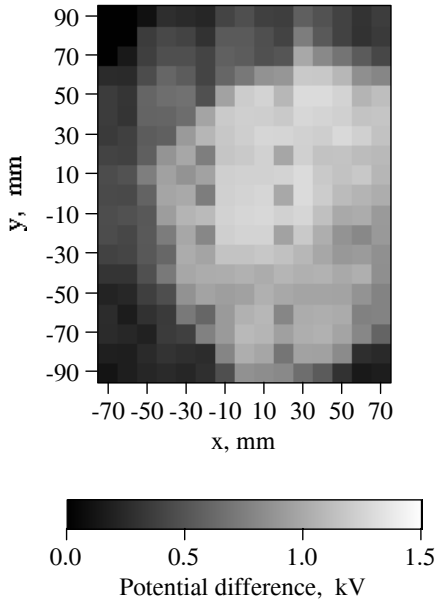

Figure 9. Distribution of potential difference at case 2.

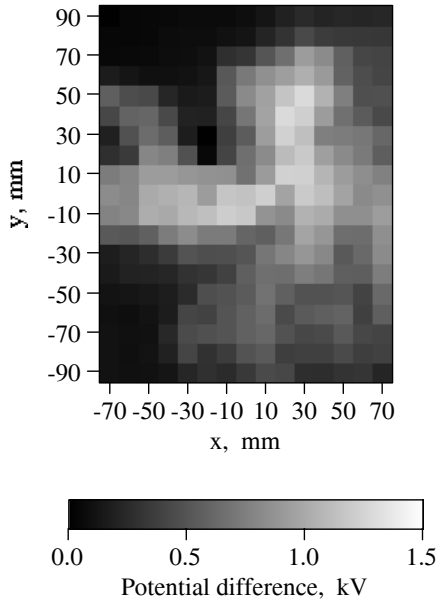

Figure 10. Distribution of potential difference at case 3.

On the basis of the potential difference measurement, the time on the inverted gradient condition is estimated as 60 hours for five years by employing NASCAP/GEO [7]. We

decided on 65 hours as the test time for coupon 3 to evaluate the power degradation due to arcing. Table 2 lists the test conditions. We tested the coupons 1 and 2 for 20 hours and the coupon 3 for 65 hours. For the cases 1~9, and case 11, the beam center was aligned to the center of the coupons. For the cases 10 and 11, the beam center was set to the center of No.1 cell of the B string, because the test purpose was to see the trigger arcs at the bus bars. The electron beam voltage, V_e was lowered gradually so that trigger arcs would occur frequently. The temporal profile of V_e was kept the same among the three test coupons. For the case 8, the external capacitance of 400 nF was used instead of 200 nF by mistake.

At every 10 hours from case 1 to 9, the coupons were removed from the chamber. After the photographs of the cell edges were taken by the 60 optical microscope, they were sent back to the factory to measure the output power. Each coupon was taken out from the vacuum chamber after the cases 2, 3, 5, 6, 8, 9, and 10. Once a coupon was put in the chamber, it was kept in vacuum for approximately three days. Every time the coupons were exposed to atmosphere, they were baked for 2 hours at 70˚C before the ESD tests.

Test Results and Discussions

In Table 3 we list the number of arcs observed. During the 20 hour experiment, the number of arcs is 288, 392, and 266, respectively for the coupons 1, 2, and 3. The coupon 2 had arcs more than the other two coupons. The cases 10 and 11 had 260 arcs in 10 hours. The cases with higher arc rates had higher chamber pressures. With so many trigger arcs, there was no sustained arc and we confirmed that the solar array design is very effective at suppressing the sustained arc occurrence.

In Figs. 9 and 10, we show the distribution of potential difference, ΔV over a coupon. The case 2 has $\emptyset_{bias}$ = -4 kV and V_e = 3 kV. The case 3 had $\emptyset_{bias}$ = -6 kV and V_e = 3.4 kV. In the both cases the potential difference is higher than 1 kV but the distribution patterns are different. For the case 2, the center of the coupon that is also the center of the beam is charged to a high potential difference more than 1 kV. In this case, the coupon surface has a potential more positive than -3 kV and the electron beam of 3 kV can reach the surface even though it is decelerated. Therefore, the coverglass surface is charged due to emission of electron-induced secondary electrons. For the case 3 where the coupon is biased to -6 kV, however, even if the potential difference is 1.5 kV, the surface potential is still -4.5 kV. Therefore, the electron beam cannot reach the surface and the surface is charged by positive ions produced by ionization of neutral gas via the electron beam.

Table 3. Number of arcs.

Case	Coupon	N_{arc}	t_{exp}, h	p, 10^{-3} Pa
1	1	78	6	1.12
2	1	78	4	1.25
3	1	132	10	0.98
4	2	58	6	1.10
5	2	1	4	0.65
6	2	333	10	2.46
7	3	60	6	0.86
8	3	41	4	0.62
9	3	165	10	0.83
10	3	150	6	2.51
11	3	110	4	1.73
12	3	84	35	0.56

In Fig. 11, we show the positions of all the arcs during the tests. Majority of the arcs occurred at the interconnectors that are exposed to space. The arc positions of cases 2 and 3 agree well with the potential distribution shown in Figs. 9 and 10. In cases 4, 5, 6, 10, and 11 many arcs are observed at the cell edges unlike other cases.

In Fig. 12, we show a typical example of arc current waveforms. This is the waveform measured by CP_{total} for an arc at an interconnector at the B string during the case 1. The pulse width is approximately 30 μs. From this kind of waveform, we identify the peak value and calculate the charge by integrating the current with respect to time. At the arc inception we also observed the jump of ionization gauge due to vaporization of the surface material near the arc spot.

Table 4 lists the results of the peak currents, the charge flown as the arc current, and the pressure increase at the arc inception. We also list the amount of charge stored in the external capacitance, $Q = C_{ext}\, jV_{bias}\, j$. The table lists the average and the standard deviation of each item. For the test using the coupon 2, we did not use the current probes that could measure up to DC. Therefore the results of the cases 4, 5, and 6 are not listed. The average of the peak current increases as the charge stored in the external capacitance increases. There is no significant difference between the coupons 1 and 3 as we compare the cases with the same external charge, Q.

After the test, we observed the power degradation for all the three coupons. In Fig. 13 we plot the ratio of degraded power to the initial power. The horizontal axis denotes the test time. The R and B strings were connected in parallel at the backside of the coupon, and were not separated as we measured the output power. The R and B strings degraded most severely, 23% in 59 arcs and 49% in 392 arcs. The coupon 1 suffered 19% degradation in 156 arcs but remained the same in 288 arcs. The coupon 3 showed little degradation up to 266 arcs but degraded severely after that. From these results, the power degradation is not simply proportional to the number of arcs. There is a certain type of trigger arc that damages the PN junction. The cell performance degrades only when such a damaging arc occurs.

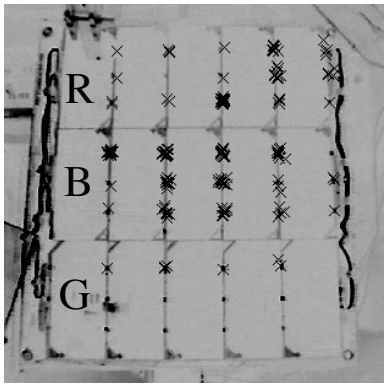

(a) Cases 1 and 2

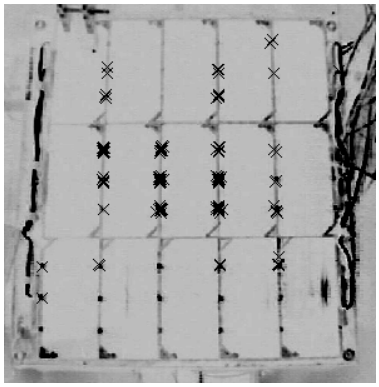

(b) Case 3

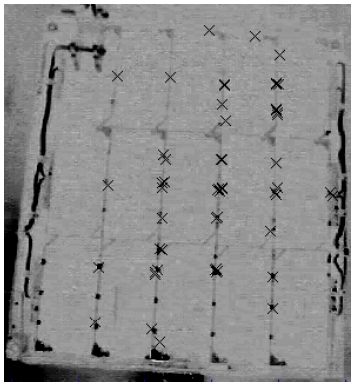

(c) Cases 4 and 5

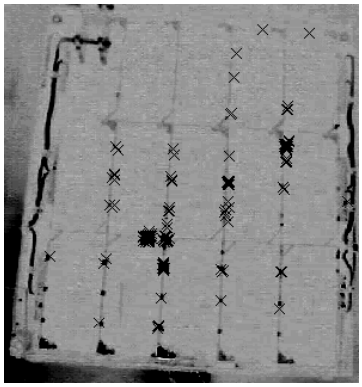

(d) Case 6

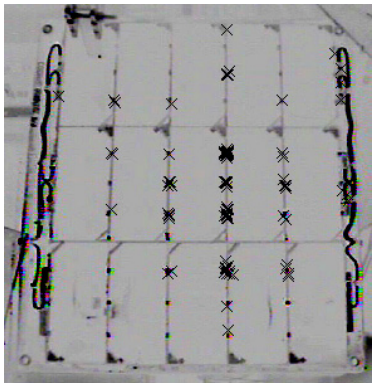

(e) Cases 7 and 8

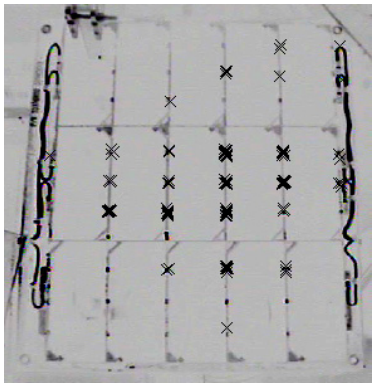

(f) Case 9

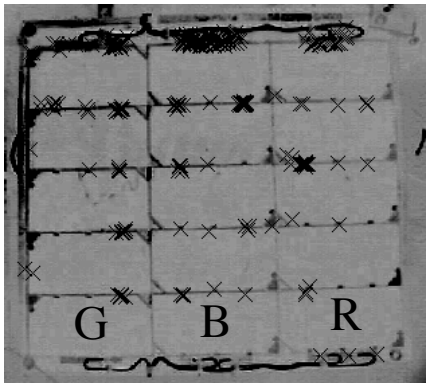

(g) Cases 10 and 11

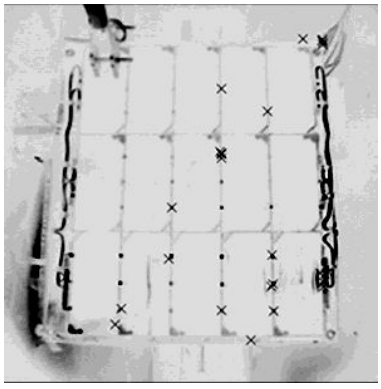

(h) Case 12

Figure 11. Positions of arcs.

Table 4. Statistics of peak current, charge, and pressure increase dore to each arc.

Case	Q, mC	I_{ave}, A	I_{std}, A	Q_{ave}, mC	Q_{std}, mC	Δp_{ave}, mPa	Δp_{std}, mPa
1	1.2	123.5	50.8	1.12	0.23	1.32	0.14
2	0.8	105.5	49.0	0.80	0.06	1.15	0.08
3	0.6	81.6	33.1	0.64	0.04	0.97	0.08
7	1.2	151.5	108.7	1.22	0.22	1.38	0.14
8	1.6	159.4	65.1	1.56	0.16	2.06	0.11
9	0.6	71.2	27.0	0.63	0.02	0.94	0.99
10	1.2	144	66.5	1.27	0.13	1.53	0.15
11	0.8	111	69.5	0.80	0.01	1.12	0.10
12	1.2	155	59.9	1.27	0.13	1.60	0.19

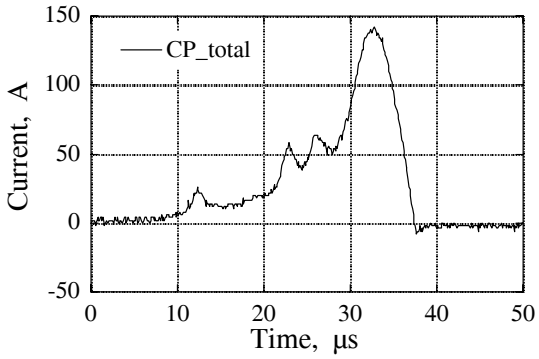

Figure 12. Typical example of arc current waveform.

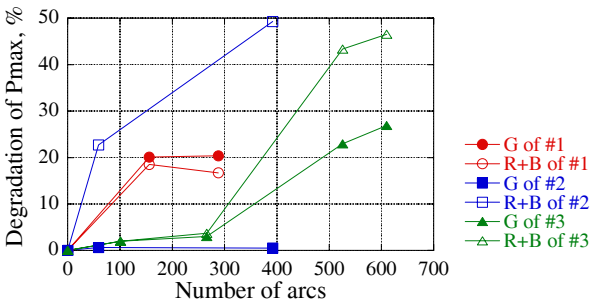

Figure 13. Degradation of solar array output power.

After the tests as for the coupon 2, the electric performance was measured with cutting the parallel connection between R and B string. The result showed that one cell in R string and two cells in B string were short-circuited. From this result, it was estimated that about 400 arcs could destroy 3 cells. From the analysis using NASCAP/GEO, the number of trigger arcs was estimated at 14950 during 5 years [7]. For WINDS satellite with 5 years lifetime, the number of the degraded cells is calculated at about 112 cells.

We identified the damaged cells of the coupon 2. The cell 2 and 4 of the B string and the cell 4 of the R string were short-circuited and generated little voltage. We carried out detailed analysis via the IR-OBIRCH method [4] on the cell 4 of the B string. The short-circuited PN junction was located at the cell edge. In Fig. 14 we show a microscope photograph of the short-circuited position taken after the test. There was an arc spot of silver color at the cell edge where the current leakage via the short-circuited PN junction was identified. The arc occurred at a void of RTV that should have covered the edge. Through the void, the cell edge was exposed to space. Trigger arcs often occurs at such void and if they occur at the cell edges they are likely to short-circuit the PN junction. It is difficult to prevent the formation of void in RTV during the manufacturing processes of solar array panels. We can fill in the void by putting additional RTV. The coupon 2 had the voids more than the other two coupons. We paid special attention to the other two coupons to inspect the cell edges and fill in the voids. Still, even for a coupon panel of 15 cells we can not completely prevent the formation of the voids. It is practically impossible to inspect all the edges of more than 8,000 cells and fill in the voids.

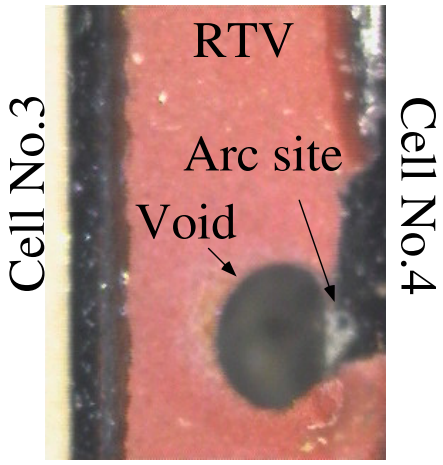

Figure 14. Photograph of the arc spot responsible for the short-circuit of PN junction of the B string of the coupon 2.

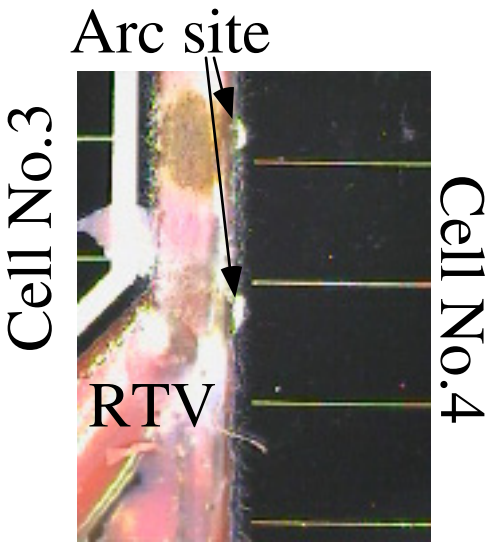

Figure 15. Photograph of the arc spot suspected to be responsible for the power degradation of the R string of the coupon 3.

In Fig. 16 we show a photograph of the cell 4 of the R string of the coupon 3 which had arcs during the case 10. There are two arc spots at the cell edge. They are very similar to the arc spot shown in Fig. 16 and probably the cause of power degradation after the last 10 hours of the coupon 3 as shown in Fig. 13. In Fig. 15, however, there is no void in RTV. The G string had a similar arc spot without a void nearby that was formed during the last 10 hours. Probably, the height of grouted RTV was not high enough to cover the conductive area at the cell edge. Therefore, the presence of void is not the necessary condition for the power degradation. The necessary condition is that a trigger arc occurs at the cell edge.

It is difficult to completely suppress the trigger arcs leading to the power degradation. Using an extra amount of RTV certainly reduces the probability of trigger arc inception. But at the same time, it increases the probability of void formation as the total volume of RTV increases. Also the more RTV coating leads to the more contamination of coverglass as reported in Ref. [4] and the more weight. Using little or no RTV increases the probability of trigger arc inception. Therefore, there is the optimum level of how much RTV coating should be used. To determine the optimum level, we need an estimate on how much the solar array output power really degrades in orbit and use the estimate as an input parameter of the system analysis.

In the first 20 hours of the test on the coupon 3, only few arcs occurred on the bus bars because the beam center was aligned with the center of the coupon. In order to see the effects of exposed bus-bars, we shifted the beam center toward the bus bar in the cases 10 and 11. During the test of total 30 hours, there was no sustained arc on the coupon 3. Therefore, exposing the bus bars does not increase the risk of the sustained arc.

In cases 10 and 11, there were 121 arcs at the bus bars. There were 137 arcs at the other parts, such as interconnectors or cell edges. Although trigger arcs occur at the bus bar as frequently as the other parts, they don't dominate the arc occurrence as we originally hoped. As long as an arc occurs at the bus bar, however, the trigger arc plasma initializes the charging processes at the other points. Therefore, the arcs at the bus bar reduces the risk of

trigger arcs at the other points, although the degree of reduction may not be so large. Nevertheless, there is no active reason for coating the bus bars with RTV, as long as exposing bus bars causes no harm.

Table 5. Arc parameters depending on arc position.

Case	Position	I_{ave}, A	I_{std}, A	Q_{ave}, mC	Q_{std}, mC
10	Bus bar	122	36	1.23	0.08
10	IC	128	34	1.24	0.09
11	Bus bar	91	37	0.79	0.05
11	IC	88	24	0.75	0.04

In Table 5 we list the peak current and the charge of the trigger arcs at the bus bars and the interconnectors for the cases 10 and 11. There is no significant difference depending on the positions. We have concluded that there is no need to coat the bus bars with RTV as long as the satellite does not carry ion thrusters.

Conclusion

We carried out the laboratory tests on solar array for WINDS. We tested three types of solar array coupons. There was no sustained arc in any coupon during the total 105 hours of the test. We observed the power degradation in all the coupons. The power degradation was caused by trigger arcs at the cell edges that were exposed to space. Coating the cell edge with RTV was not a prefect solution because there were always voids in the RTV.

Exposing the bus bars to space without any coating with RTV did not show any side-effect. Therefore, to reduce the satellite mass and reduce the risk of arcs at the cell edge, we determined not to coat the bus bars with RTV.

We summarize the flight design of WINDS solar array in the following;

1. To suppress the inter-string sustained arc, the gap between strings is grouted with RTV.
2. To suppress the string-substrate sustained arc, the RTV layer between the cells and the Kapton sheet is specified as 100 μm and the RTV layer leaks out at the cell gap in the direction of series connection.
3. There is no coating of bus bar with RTV.
4. To avoid trigger arcs at the cell edges, we give the best effort to fill in the voids of RTV by additional RTV.

In the present test, the power degradation due to trigger arcs was also confirmed for triple-junction cells in addition to Si cells tested in Ref. [4]. We also found that the necessary condition for the power degradation is trigger arcs at the cell edge. We still don't know how large the trigger arc must be to cause the damage. In the present test, we assumed that the electrostatic energy stored in the entire paddle of solar array would be given to each trigger arc plasma. Whether this is really true or not is still under controversy and the present test was carried out assuming the worst case. In future we need to study the threshold of the trigger arc energy for the power degradation and whether such energy is really available for a trigger arc in orbit.

References

1. Hastings, D. E. and Garrett, H. : Spacecraft Environmental Interactions, Cambridge Univ. Press, 1996.

2. Katz, I. , Davis, V.A. and Snder, D.B. : Mechanism for Spacecraft Charging Initiated Destruction of Solar Arrays in GEO, AIAA 98-1002, 36th Aerospace Sci. Meeting, (1998).

3. Cho, M., Matsumot, T., Ramasamy, R., Toyoda, K., Nozaki, Y. Takahashi, M.: Laboratory Tests on 110V Solar Arrays in a Simulated Geosynchronous Orbit Environment AIAA 2002-0630, 40th Aerospase Sciences Meeting, Reno, January, 2002

4. Toyoa, K., Matsumoto, T., Cho, M., Nozaki, Y., and Takahashi, M.: Power reduction of solar arrays due to arcing under simulated GEO environment AIAA 2003-0682, 41st Aerospace Science Meeting, Reno, January, 2003.

5. Leung, P.: Plasma Phenomena Associated with Solar Array Discharges and Their Role in Scaling Coupon Test Results to a Full Panel AIAA 2002- 0628, 40th Aerospase Sciences Meeting, Reno, January, 2002

6. Toyoda, K., Cho, M., and Hikita, M.: Development of Position Identitifcation System of Arc Discharge on a Solar Array in Vacuum by Digital Processing of Video Images, J. Japan Soc. Aero. Space Sci.,Vol.51, No.589, pp.82-84, 2003.

7. Sato, T., Takahashi, M., Nakamura, M., Kawakita, S., Cho, M., Toyoda, K., and Nozaki, Y.: Development of Solar Array for a Wideband Internetworking Engineering Test and Demonstration Satellite: System Design, 8th Spacecraft Charging Technology Conference, Huntsville, USA, October, 2003.